Hindawi
Stem Cells International
Volume 2020, Article ID 9369268, 12 pages
https://doi.org/10.1155/2020/9369268

Research Article

Changes in the Expression of Mitochondrial Morphology-Related Genes during the Differentiation of Murine Embryonic Stem Cells

Jeong Eon Lee,[1] Bong Jong Seo,[1] Min Ji Han,[1] Yean Ju Hong,[1] Kwonho Hong,[1] Hyuk Song,[1] Jeong Woong Lee,[2] and Jeong Tae Do[1]

[1]*Department of Stem Cell and Regenerative Biotechnology, KU Institute of Science and Technology, Konkuk University, 120 Neungdong-ro, Gwangjin-gu, Seoul 05029, Republic of Korea*
[2]*Biotherapeutics Translational Research Center, Korea Research Institute of Bioscience and Biotechnology, Daejeon 305-806, Republic of Korea*

Correspondence should be addressed to Jeong Tae Do; dojt@konkuk.ac.kr

Jeong Eon Lee and Bong Jong Seo contributed equally to this work.

Received 22 August 2019; Revised 17 December 2019; Accepted 7 January 2020; Published 28 January 2020

Academic Editor: Heinrich Sauer

During embryonic development, cells undergo changes in gene expression, signaling pathway activation/inactivation, metabolism, and intracellular organelle structures, which are mediated by mitochondria. Mitochondria continuously switch their morphology between elongated tubular and fragmented globular via mitochondrial fusion and fission. Mitochondrial fusion is mediated by proteins encoded by *Mfn1*, *Mfn2*, and *Opa1*, whereas mitochondrial fission is mediated by proteins encoded by *Fis1* and *Dnm1L*. Here, we investigated the expression patterns of mitochondria-related genes during the differentiation of mouse embryonic stem cells (ESCs). Pluripotent ESCs maintain stemness in the presence of leukemia inhibitory factor (LIF) via the JAK-STAT3 pathway but lose pluripotency and differentiate in response to the withdrawal of LIF. We analyzed the expression levels of mitochondrial fusion- and fission-related genes during the differentiation of ESCs. We hypothesized that mitochondrial fusion genes would be overexpressed while the fission genes would be downregulated during the differentiation of ESCs. Though the mitochondria exhibited an elongated morphology in ESCs differentiating in response to LIF withdrawal, only the expression of *Mfn2* was increased and that of *Dnm1L* was decreased as expected, the other exceptions being *Mfn1*, *Opa1*, and *Fis1*. Next, by comparing gene expression and mitochondrial morphology, we proposed an index that could precisely represent mitochondrial changes during the differentiation of pluripotent stem cells by analyzing the expression ratios of three fusion- and two fission-related genes. Surprisingly, increased *Mfn2*/*Dnm1L* ratio was correlated with elongation of mitochondria during the differentiation of ESCs. Moreover, application of this index to other specialized cell types revealed that neural stems cells (NSCs) and mouse embryonic fibroblasts (MEFs) showed increased *Mfn2*/*Dnm1L* ratio compared to ESCs. Thus, we suggest that the *Mfn2*/*Dnm1L* ratio could reflect changes in mitochondrial morphology according to the extent of differentiation.

1. Introduction

During embryonic development, cells undergo various changes in gene expression [1, 2] and signaling pathways [3]. Metabolism and intracellular organelle structures are also altered during development and differentiation [4–6]. Specifically, the organellar changes are observed during the regaining of pluripotency (also known as reprogramming) [7]. For example, Folmes et al. showed that the globular shape of mitochondria progressively changed to elongated during embryonic development from zygote to somite embryo. Accordingly, metabolic features such as pyruvate oxidation, glucose oxidation, glycolysis, and the pentose phosphate pathway (PPP) were also changed dynamically [6]. These features return to the developmental early-stage status during the reprogramming process [8]. Some of the

most dramatic changes in cells during development and differentiation occur in the mitochondria, which play essential roles in cellular processes, including energy metabolism [9], apoptosis [10], aging [11], reactive oxygen species production, calcium homeostasis, and differentiation [12].

Mitochondria continuously change their morphology through fusion and fission in response to cellular requirements, which is the crux of mitochondrial quality control. In addition, mitochondria increase their population through self-division from the existing mitochondria; this is called mitochondrial biogenesis [13–16]. Mitochondrial dynamics and biogenesis vary by cell type and cellular environment. In addition, the quality and quantity of mitochondria can affect the cellular behavior and play a pivotal role in cell metabolism [17].

In preimplantation embryonic and pluripotent stem cells, immature mitochondria characterized by a small and globular shape with poorly developed cristae are observed [14, 18, 19]. Cells with immature mitochondria show low oxygen consumption and high levels of glycolytic enzymes [20]. Thus, undifferentiated embryonic stem cells (ESCs) also exhibit low levels of ATP production, modest levels of antioxidant enzymes, and poor oxidant capacity [14, 19, 20]. Upon differentiation of ESCs, mitochondria in these cells become elongated, showing developed cristae and dense matrices [21]; this results in high oxygen consumption and ATP production for more efficient cellular activity [14, 18, 19].

In mammals, mitochondrial morphology switches between elongated tubular and fragmented globular by fusion and fission, respectively [22, 23]. Mitochondrial fusion is mediated by the dynamin family GTPases, such as mitofusin (MFN) 1, MFN2, and optic atrophy 1 (OPA1) [24–26]. Although the exact fusion mechanism has yet to be defined, MFN1 and MFN2 form a dimer that inserts itself into the mitochondrial outer membrane, whereas OPA1 is located in the mitochondrial inner membrane [27, 28]. MFN1, MFN2, and OPA1 contain a GTPase domain, hydrophobic heptad repeat (HR) domain, and transmembrane domain [24, 29]. MFN1 and MFN2 play similar roles in mitochondrial fusion and thus can functionally replace each other and form homotypic or heterotypic dimers [25, 30].

In contrast, the major proteins related to mitochondrial fission are FIS1 [31–33] and dynamin-related protein 1 (DNM1L, also called DRP1) [34–36]. DNM1L is mainly located in the cytosol and recruited to the outer membrane of the mitochondria where it induces fission [30]. FIS1 is located in the outer mitochondrial membrane and is closely related to DNM1L [32, 33]. DNM1L can interact with other mitochondrial fission proteins, including mitochondrial fission factor (MFF) and FIS1. Interestingly, a recent study suggested that DNM1L can interact with the fusion protein MFN and facilitate MFN-mediated fusion [30]. Although many studies have evaluated the fusion and fission of mitochondria, the mechanisms and signaling pathways that determine mitochondrial dynamics are still unclear. Activation of the mammalian target of rapamycin (mTOR) pathway by the withdrawal of LIF induced mouse ESC differentiation with suppression of pluripotent genes such as *Klf4*, *Oct4*, and *Nanog* [37]. When pluripotent stem cells differentiate, they require more energy to meet the demands of their newly acquired functions [6].

Accordingly, mitochondria undergo dynamic remodeling during differentiation, and thus, mitochondrial morphology and metabolism are changed. Therefore, we hypothesized that expression of mitochondrial fusion- and fission-related genes may be changed toward a certain direction during the spontaneous differentiation of ESCs. Here, we quantified the expression levels of the fusion-related genes *Mfn1*, *Mfn2*, and *Opa1* and the fission-related genes *Fis1* and *Dnm1L* during the differentiation of murine ESCs. Here, we investigated these genes to determine whether they could be used as an index of the extent of differentiation and changes in mitochondrial morphology.

2. Materials and Methods

All methods used in this study were carried out in accordance with animal care and use guidelines, and all experimental protocols were approved by the Institutional Animal Care and Use Committee of Konkuk University.

2.1. Cell Cultures. Mouse ESCs (E14tg2a) were purchased from the American Type Culture Collection (ATCC, Manassas, VA, USA) and cultured on culture dishes layered with inactivated MEFs in an ESC medium, consisting of Dulbecco's modified Eagle's medium (DMEM; Gibco) supplemented with 15% fetal bovine serum (FBS; HyClone), 1× Penicillin/Streptomycin/Glutamine (P/S/G; Gibco), 0.1 mM nonessential amino acids (NEAAs; Gibco), and 1 mM β-mercaptoethanol (Gibco) with 1000 U/mL leukemia inhibitory factor (ESGRO, Chemicon International). MEFs were cultured in culture dishes coated with 0.15% porcine gelatin (Sigma, St. Louis, MO, USA) in MEF medium consisting of DMEM (Gibco) supplemented with 15% FBS (HyClone), 1x P/S/G (Gibco), 0.1 mM NEAAs (Gibco), and 1 mM β-mercaptoethanol (Gibco). NSCs were cultured in culture dishes coated with 0.15% porcine gelatin (Sigma) in NS medium consisting of DMEM : Nutrient Mixture F-12 (Gibco), 0.5 mg/mL bovine serum albumin (BSA; Sigma), 1% N2 supplement (Gibco), 1x NEAAs (Gibco), 1x P/S/G (Gibco), 10 ng/mL basic fibroblast growth factor (bFGF; R&D systems), and 10 ng/mL epidermal growth factor (EGF; Gibco). All cell lines were incubated at 37°C in an atmosphere of 5% CO_2 and maintained on tissue culture dishes (Corning, Amsterdam, The Netherlands).

2.2. In Vitro Differentiation. Pluripotent ESCs maintain stemness in the presence of LIF via the JAK-STAT3 pathway. However, when this pathway is inhibited in response to LIF withdrawal, pluripotent ESCs randomly differentiate into endodermal, ectodermal, and mesodermal cells. Cherepkova et al. showed that LIF withdrawal induced mouse ESC differentiation via the activation of the mTOR pathway [37]. Based on the differentiation protocol, we have established an ESC differentiation protocol that has been customized for our laboratory conditions. In the preplating process, ESCs cultured with feeder cells were dissociated by trypsin-EDTA (0.25%) (Gibco) and transferred to a 0.15% gelatin-coated dish and

Table 1: Primer sets used for quantitative RT-PCR.

Gene	Forward	Reverse
Mfn1	5′-CATGGGCATCATGGTTGTTGGG-3′	5′-TCTCCACTGCTCGGGTGTAG-3′
Mfn2	5′-CAAGTGTCCGCTCCTGAAGG-3′	5′-GAACCTCCTTGGCAGACACG-3′
Opa1	5′-CAAGCATTACAGGAAGGTGTCAGAC-3′	5′-CACTGAGAGTCACCTTCACTGG-3′
Fis1	5′-CATCGTGCTGCTGGAGAGC-3′	5′-GCAGAGAGCAGGTGAGGCTG-3′
Dnm1L	5′-GGAGTTGAAGCAGAAGAATGGGG-3′	5′-CAGTGACGGCGAGGATAATGG-3′
Oct4	5′-GATGCTGTGAGCCAAGGCAAG-3′	5′-GGCTCCTGATCAACAGCATCAC-3′
Nanog	5′-CTTTCACCTATTAAGGTGCTTGC-3′	5′-TGGCATCGGTTCATCATGCTAC-3′
T	5′-CCGGTGCTGAAGGTAAATGT-3′	5′-CCTCCATTGAGCTTGTTGGT-3′
Actb	5′-CGCCATGGATGACGATATCG-3′	5′-CGAAGCCGGCTTTGCACATG-3′

incubated at 37°C in an atmosphere of 5% CO_2 for 2 h to remove the feeder cells. Because the feeder cells attached to the gelatin-coated dish much earlier than ESCs, the supernatant of the culture mostly contains ESCs without contamination of feeder cells. The supernatant was transferred to another gelatin-coated dish and used as the differentiation experiment. For *in vitro* differentiation, 1×10^5 ESCs were seeded in 100 mm cell culture dishes coated with 0.15% porcine gelatin (Sigma) with MEF medium. The medium was refreshed every day for 15 days of differentiation. The cells were collected by scraping for experimental analysis.

2.3. RNA Isolation and qRT-PCR. Total RNA was isolated using TRIzol reagent (Invitrogen, Carlsbad, CA, USA) according to the manufacturer's protocol. The cDNA was then synthesized from 1 mg total RNA using SuperScript III Reverse Transcriptase (Invitrogen) and oligo(dT)20 primer (Invitrogen) according to the manufacturer's instructions. qPCR was performed in duplicate with Power SYBR Green Master Mix (Takara, Shiga, Japan), and results were analyzed on a Roche LightCycler 5480 (Roche). Thermal cycling was carried out via 45 cycles of 10 s at 95°C, 10 s at 60°C, and 20 s at 72°C. The primers for qRT-PCR are shown in Table 1. Gene expression levels were normalized to those of *Actb*.

2.4. Western Blot Analysis. Total cells were lysed using RIPA buffer (Thermo Fisher) according to the manufacturer's instructions. Cell lysates (20 μg protein) were separated on NuPAGE 4–12% Bis-Tris Gels (Invitrogen) and transferred to polyvinyl difluoride membranes. The membranes were blocked using a blocking solution containing 5% skim milk powder and 0.05% Tween 20 in phosphate-buffered saline (PBS). The primary antibodies used in this study were as follows: anti-OCT4 (rabbit, 1 : 1000; Santa Cruz Biotechnology, Santa Cruz, CA, USA), anti-Nanog (rabbit, 1 : 1000; Abcam, Cambridge, UK), anti-MFN2 (mouse, 1 : 1000; Abcam), anti-DRP1 (rabbit, 1 : 1000; Millipore), anti-MFN1 (mouse, 1 : 1000; Abcam), anti-FIS1 (mouse, 1 : 500; Abcam), and anti-β-actin (mouse, 1 : 10000; Sigma). The membranes were incubated with these antibodies overnight at 4°C. Secondary antibodies were conjugated with anti-mouse IgG-peroxidase (1 : 10000; Sigma), anti-goat IgG-horseradish peroxidase (HRP), and anti-rabbit IgG-HRP (1 : 10000; Santa Cruz Biotechnology), and the membranes were incubated with these antibodies for 90 min at room temperature.

Antigens were detected using Pierce ECL Western Blotting chemiluminescent substrate (Thermo Fisher), according to the manufacturer's instructions. Blots were then exposed to X-ray film for development and stripped for reuse of the membranes. Anti-β-actin antibody (mouse, 1 : 10000; Sigma) was used as a control. Densitometry of the bands for the proteins and their loading controls was performed using ImageJ 1.43 (NIH) software. Protein expression levels were normalized to those of *Actb*.

2.5. Immunocytochemistry. For immunocytochemistry, cells were fixed with 4% paraformaldehyde for 20 min at room temperature. The cells were washed with PBS and then treated with PBS containing 3% bovine serum albumin and 0.03% Triton X-100 for 30 min at room temperature. The cells were then incubated with the following primary antibodies: anti-OCT4 (1 : 500; Santa Cruz Biotechnology), anti-Nanog (1 : 200; Abcam), anti-βIII-tubulin (TUJ1; 1 : 500; R&D), anti-SMA (1 : 200; Abcam), anti-SOX17 (1 : 300; R&D), and anti-TOM20 (1 : 200; Santa Cruz Biotechnology). Fluorescently labeled (Alexa Fluor 488 or 647; Abcam) secondary antibodies were used according to the manufacturer's specifications. Images for anti-TOM20 staining were obtained with a confocal microscope (Zeiss).

2.6. Electron Microscopy. For transmission electron microscope (TEM) experiments, the samples were fixed in 4% paraformaldehyde (Sigma) and 2.5% glutaraldehyde (Sigma) in 0.1 M phosphate (Sigma) buffer for 24 h. After washing in 0.1 M phosphate buffer, the samples were postfixed for 1 h in 1% osmium tetroxide (Sigma) prepared in the same buffer. The samples were dehydrated with a graded series of ethyl alcohol concentrations, embedded in Epon 812, and polymerized at 60°C for 3 days. Ultrathin sections (60–70 nm) were obtained using an ultramicrotome (Leica Ultracut UCT), collected on grids (200 mesh), and examined under a TEM (JEM 1010) operating at 60 kV, and images were recorded by a charge-coupled device camera (SC1000; Gatan).

2.7. Mitochondrial Length Analysis. The images from electron microscopy were analyzed and measured by the ImageJ 1.43 (NIH) software for calculating the maximum (Max)/minimum/(Min) ratio of mitochondrial length. At least over fifty mitochondria were measured and analyzed per sample to obtain data.

2.8. Statistical Analysis. All experiments were performed in triplicate, and data are presented as mean ± standard error of mean (SEM). Differences were assessed using one-way ANOVA with Tukey's honestly significant difference (HSD) post hocs or Fisher's least significant different (LSD) post hocs for multiple comparisons appropriately, and differences with p values of less than 0.05 were considered significant.

3. Results

3.1. Changes in Pluripotency- and Tissue-Specific Markers during the Differentiation of Mouse ESCs. To examine changes in gene expression during the differentiation of ESCs, we randomly differentiated mouse ESCs by the withdrawal of LIF without feeder cells for 0, 3, 6, 9, 12, and 15 days (Figure 1(a)). Dome-like colonies of undifferentiated ESCs became flat and showed changes in morphology. First, we checked whether ESCs were properly differentiated *in vitro* after 15 days in differentiation medium. Immunocytochemistry analysis showed that Oct4 and Nanog, which were expressed in undifferentiated ESCs, were silenced at day 15 after differentiation. Differentiation markers, neuron-specific class III β-tubulin (Tuj1), smooth muscle actin (SMA), and SRY-box 17 (Sox17) for ectodermal, mesodermal, and endodermal cells, respectively, were not detectable in undifferentiated ESCs at day 0 but were detected after differentiation at day 15, indicating that ESCs lost pluripotency and were differentiated into various cell types, including all three germ layers (Figure 1(b)).

Next, we evaluated the expression levels of pluripotency and differentiation markers by quantitative reverse transcription polymerase chain reaction (qRT-PCR) analysis (Figures 1(c) and 1(d)). The expression levels of the pluripotency markers *Oct4* ($F = 34.18$, $p < 0.001$) and *Nanog* ($F = 1927.49$, $p < 0.001$) were gradually decreased as ESCs were differentiated (Figure 1(c)). In contrast, early mesoderm marker *T* (also known as Brachyury) (one-way ANOVA with Tukey's HSD, $F = 455.71$, $p < 0.001$) expression was increased until day 6 postdifferentiation and then downregulated afterward (Figure 1(d)), indicating that early mesoderm cells appeared at day 6 after differentiation and then differentiated further. Taken together, our findings demonstrated that ESCs differentiated gradually and lost pluripotency over 15 days upon LIF withdrawal from the ESC medium.

3.2. Changes in Mitochondrial Morphology during the Differentiation of Mouse ESCs. Mitochondrial morphology was expected to change from fragmented to elongated shapes during the differentiation of ESCs. At first, we investigated the mitochondrial biogenesis by immunostaining using antibodies targeting translocase of the outer membrane 20 (TOM20), which is in the outer mitochondrial membrane during the differentiation of ESCs. In ESCs, mitochondria (green dots in Supplementary Fig. 1) were evenly distributed in the cytoplasm. However, the number of green dots had been increased since the differentiation of ESCs (Supplementary Fig. 1). Next, we observed the mitochondrial morphologies accurately by electron microscopic analysis during the differentiation of ESCs (Figure 2(a)). Undifferentiated ESCs had primarily globular mitochondria with immature cristae, and this morphology was maintained until day 3 of differentiation. From days 6 to 15, mitochondria were gradually elongated and showed mature cristae (Figure 2(a)). We measured the Max and Min axes of mitochondria (one-way ANOVA with Tukey's HSD, Max: $F = 24.25$, $p < 0.001$; Min: $F = 31.87$, $p < 0.001$) to quantify mitochondrial length (Figures 2(b) and 2(c)) including mitochondrial perimeter and area (Supplementary Fig. 2a-b). The Max/Min ratios of mitochondria (one-way ANOVA with Tukey's HSD, $F = 27.10$, $p < 0.001$) were 1.51, 1.66, 3.65, 3.92, 4.30, and 6.87 on days 0, 3, 6, 9, 12, and 15, respectively (Figure 2(d)). These data clearly demonstrated that the globular and immature mitochondria in ESCs became elongated and showed developed mature cristae after the spontaneous differentiation.

3.3. Changes in Mitochondrial Morphology-Related Genes during the Differentiation of Mouse ESCs. Because mitochondria were elongated during the differentiation of ESCs, we predicted that fusion-related genes would be upregulated and fission-related genes would be downregulated during this differentiation. Thus, we examined mitochondrial morphology-related genes by qRT-PCR analysis. Unexpectedly, the fusion-related gene *Mfn1* (one-way ANOVA with Tukey's HSD, $F = 604.95$, $p < 0.001$) was progressively downregulated, whereas *Mfn2* (one-way ANOVA with Tukey's HSD, $F = 11.10$, $p < 0.001$) and *Opa1* (one-way ANOVA with Tukey's HSD, $F = 85.53$, $p < 0.001$) expression patterns fluctuated at day 3 postdifferentiation (Figure 3(a)). Next, we evaluated the expression of two fission-related genes, *Dnm1L* and *Fis1* (Figure 3(b)); consistent with the reduced mitochondrial fission, which resulted in enhanced mitochondrial elongation, the expression of Dnm1L (one-way ANOVA with Tukey's HSD, $F = 385.64$, $p < 0.001$) decreased as mouse ESCs underwent spontaneous differentiation (Figure 3(b)). However, *Fis1* (one-way ANOVA with Tukey's HSD, $F = 2.57$, $p = 0.083$) expression did not decrease but rather increased after slight downregulation at the beginning of differentiation (Figure 3(b)). This result supported previous findings that FIS1 is less related to mitochondrial fission than DNM1L and functions to recruit DNM1L to the mitochondria [38, 39]. Collectively, our results showed that *Mfn2* and *Dmn1L* mRNA expression levels reflected mitochondrial elongation with ESC differentiation.

Accordingly, we next investigated the levels of MFN2 and DNM1L proteins by western blotting in ESCs (day 0) and in differentiated cells on days 0, 3, 6, 9, 12, and 15 (Figure 3(d)). As a control for ESC spontaneous differentiation, the expression of the pluripotency marker OCT4 gradually decreased during differentiation and was almost undetectable at day 15. MFN2 was expressed at a low level in ESCs but showed a dramatic increase in expression upon

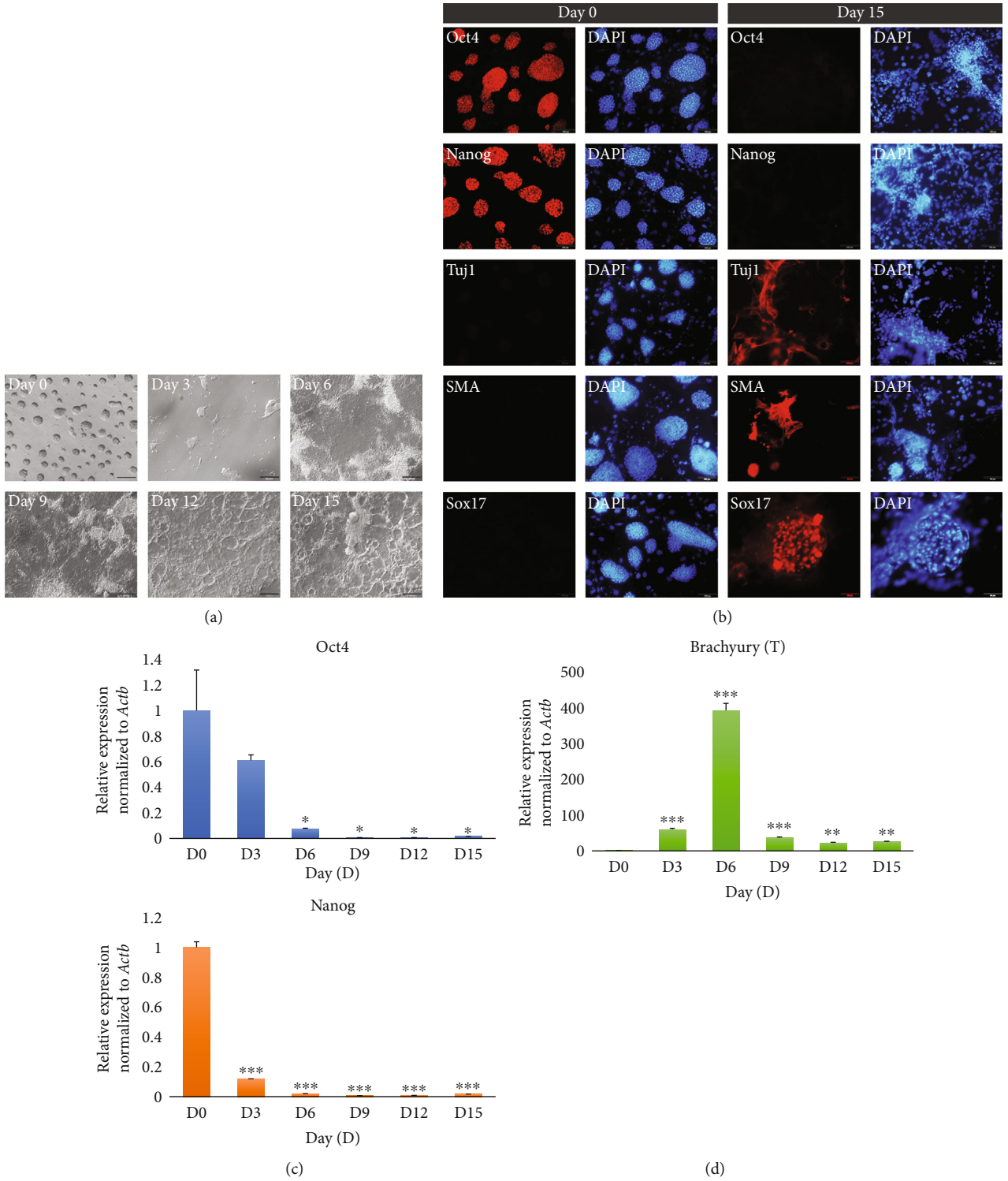

Figure 1: *In vitro* differentiation and characterization of ESCs. (a) Phase-contrast images of ESCs and differentiating cells on days 0, 3, 6, 9, 12, and 15. Scale bars = 200 μm. (b) Immunofluorescence images of the pluripotency markers Oct4 and Nanog and differentiation markers for ectodermal (Tuj1), mesodermal (SMA), and endodermal (Sox17) cells in undifferentiated ESCs and ESC-derived differentiated cells on days 0 and 15. Nuclei was counterstained with DAPI. Scale bars = 100 μm. (c, d) Quantitative RT-PCR analysis of ESCs and differentiating cells on days 0, 3, 6, 9, 12, and 15 (D0, D3, D6, D9, D12, and D15). Data are presented as mean ± SEM for $n = 3$ independent experiments. (c) Pluripotent marker *Oct4* and *Nanog* expression on days 0 to 15. (d) Differentiation marker *T* expression from days 0 to 15. $^{*}p < 0.05$, $^{**}p < 0.01$, and $^{***}p < 0.001$ versus D0.

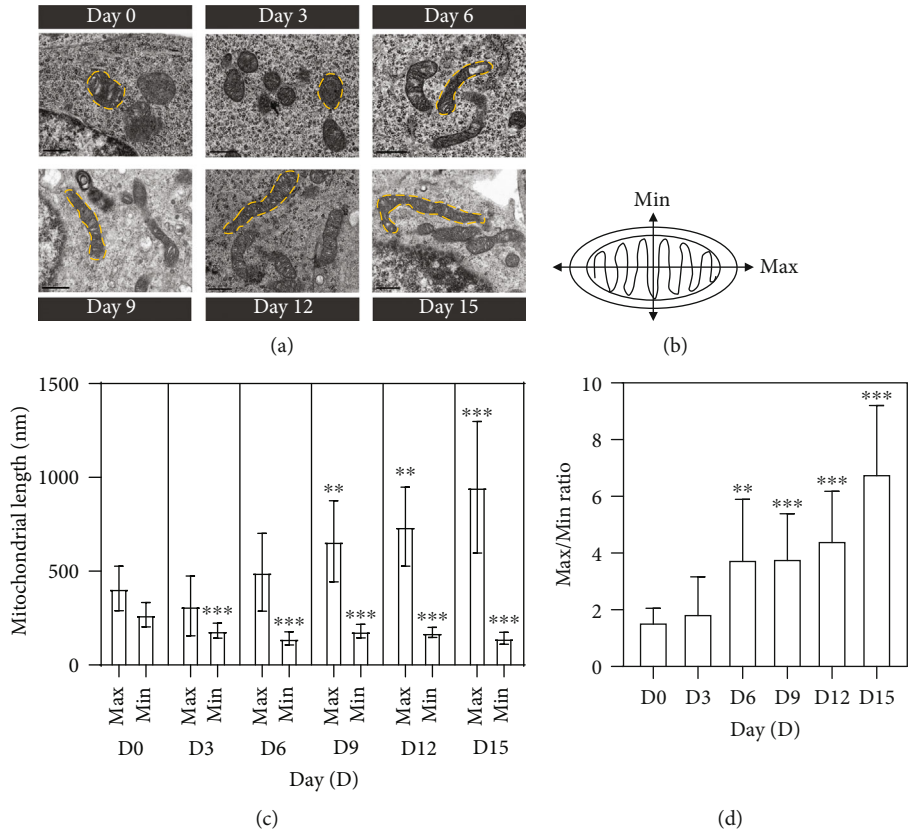

Figure 2: Changes in mitochondrial morphology during the differentiation of ESCs. (a) Electron microscopy images of mitochondria in undifferentiated ESCs and in cells differentiated from ESCs on days 0, 3, 6, 9, 12, and 15. Yellow dotted lines represent mitochondrial morphologies. Scale bars = 0.5 μm. (b) Measurement of the maximum (Max) and minimum (Min) axes of mitochondria. (c) The mitochondrial length (nm) in ESCs on days 0, 3, 6, 9, 12, and 15 of differentiation (quantified $n = 128$ from 21 cells of day 0, 28 cells of day 3, 16 cells of day 6, 15 cells of day 9, 15 cells of day 12, and 17 cells of day 15). (d) The Max/Min ratios in ESCs and differentiating cells on days 0, 3, 6, 9, 12, and 15. Data are presented as mean ± SEM for an experiment. $^{*}p < 0.05$, $^{**}p < 0.01$, and $^{***}p < 0.001$ versus D0.

spontaneous differentiation. Furthermore, MFN2 protein levels showed a fluctuating expression pattern during differentiation, similar to the qRT-PCR data (Figures 3(a) and 3(d)). DNM1L protein levels decreased gradually during the differentiation of ESCs, similar to the result of qRT-PCR analysis (Figures 3(b) and 3(d)). Thus, we observed similar changes in the mRNA and protein levels for these two targets.

3.4. Establishment of Indexes Representing the Extent of Differentiation. Given that many genes involved in mitochondrial fusion and fission are not correlated with mitochondrial morphology, we next attempted to find an index to represent mitochondrial morphology. Based on the qRT-PCR data, we analyzed the ratios between three fusion- and two fission-related genes during the differentiation of ESCs. A total of 6 combinatorial ratios for three fusion- and two fission-related genes were analyzed (Figure 3(c)). One of these, the *Mfn2*/*Dnm1L* ratio (one-way ANOVA with Tukey's HSD, $F = 31.24$, $p < 0.001$), was interesting because it was similar to the mitochondrial length Max/Min ratio during the differentiation of ESCs (Figures 2(d) and 3(c) in red square). For further evaluation, we conducted correlation analysis of *Mfn2*/*Dnm1L* ratio and mitochondrial length (Supplementary Fig. 3a). Next, we confirmed the protein expression level in the *MFN2*/*DNM1L* ratio (one-way ANOVA with Tukey's HSD, $F = 25.56$, $p < 0.001$) (Figure 3(e), Supplementary Fig. 4). Indeed, the MFN2/DNM1L ratio was also similar to the mRNA expression and mitochondrial length Max/Min ratio. Thus, we concluded that the mitochondrial changes during ESC spontaneous differentiation could be reflected by the progressive increase in the *Mfn2*/*Dnm1L* ratio.

3.5. Mfn2/Dnm1L Index Represented Mitochondrial Morphology according to the Extent of Differentiation. To investigate whether this index was applicable to other cell types, we compared this ratio among ESCs, neural stem cells (NSCs), and mouse embryonic fibroblasts (MEFs). We chose these cell types because ESCs are undifferentiated, NSCs are less specialized, and MEFs are differentiated. Only ESCs express high levels of *Oct4* (one-way ANOVA with Fisher's LSD, $F = 33.18$, $p < 0.001$) and *Nanog* (one-way ANOVA with Fisher's LSD, $F = 2051.34$, $p < 0.001$) (Figure 4(b)). Although the mRNA expression level of the mitochondrial fusion-related gene *Mfn2* (one-way ANOVA with Fisher's LSD, $F = 7.12$, $p < 0.05$) was slightly changed in these cell types, the mRNA expression level of the mitochondrial

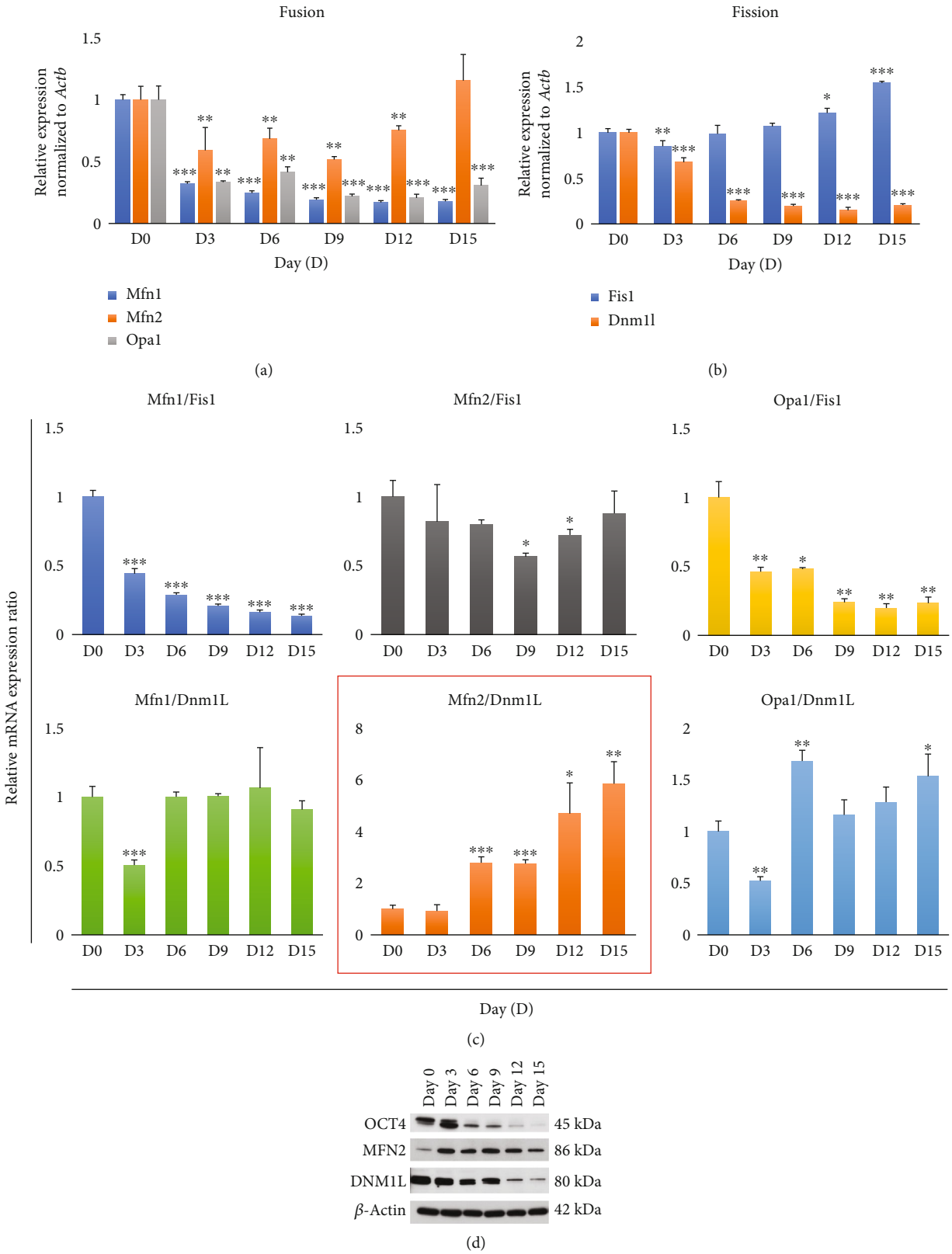

Figure 3: Continued.

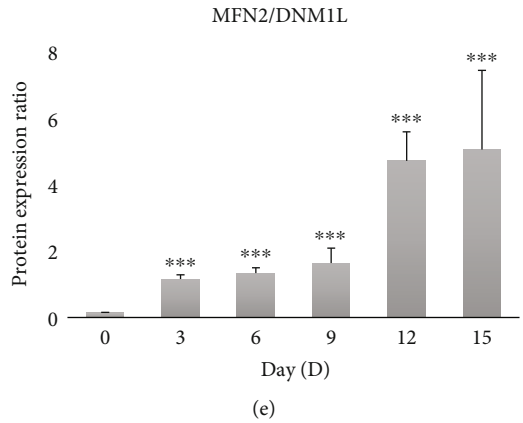

Figure 3: Changes in the expression levels of mitochondrial fusion- and fission-related genes and in indexes from combinations of fusion- and fission-related genes. Quantitative RT-PCR analysis of (a) mitochondrial fusion-related genes (*Mfn1*, *Mfn2*, and *Opa1*) and (b) mitochondrial fission-related genes (*Fis1* and *Dnm1L*) on days 0, 3, 6, 9, 12, and 15 after differentiation of ESCs. Gene expression levels were normalized to those of *Actb*. (c) Six combinatorial ratios from the analysis of gene expression levels between three fusion and two fission genes. (d) Western blotting for the expression of OCT4, MFN2, and DNM1L. β-Actin was used as a control for other proteins. (e) MFN2/DNM1L protein ratios were gradually increased according to the elapsed time after ESC differentiation. All data are presented as mean ± SEM for $n = 3$ independent experiments. $^{*}p < 0.05$, $^{**}p < 0.01$, and $^{***}p < 0.001$ versus D0.

fission-related gene *Dnm1L* (one-way ANOVA with Fisher's LSD, $F = 804.07$, $p < 0.001$) was gradually decreased in NSCs and MEFs (Figures 4(c) and 4(d)), consistent with the observed changes in mitochondrial morphology (Figure 4(a)). Next, we applied the *Mfn2*/*Dnm1L* ratio (one-way ANOVA with Fisher's LSD, $F = 50.42$, $p < 0.001$) to these cell types, with adjustment to a ratio of 1.0 for ESCs. Interestingly, the adjusted *Mfn2*/*Dnm1L* ratios were 1.0, 2.97, and 3.86 in ESCs, NSCs, and MEFs, respectively. Next, we also confirmed MFN2 and DNM1L protein expression (Figure 4(f)). As expected, the DNM1L protein expression levels were decreased in NSCs and MEFs, compared with those in ESCs. Interestingly, the MFN2 protein expression levels were gradually increased in NSCs and MEFs. The *MFN2*/*DNM1L* protein expression ratios (one-way ANOVA with Fisher's LSD, $F = 19660.5$, $p < 0.001$) were 0.16, 2.94, and 4.61 in ESCs, NSCs, and MEFs, respectively. Thus, we concluded that the *Mfn2*/*Dnm1L* ratio at the mRNA and protein expression levels corresponded to the length of mitochondria (Figures 4(e)–4(g)).

4. Discussion

In this study, we investigated the dynamics of mitochondrial morphology-related genes, which are responsible for mitochondrial fusion and fission, during the differentiation of mouse ESCs. Given that differentiated cells contain elongated mitochondria and ESCs contain globular mitochondria [9], we expected to observe increases in the expression of mitochondrial fusion-related genes (*Mfn1*, *Mfn2*, and *Opa1*) and decreases in the expression of fission-related genes (*Fis1* and *Dnm1L*).

This is because several reports have shown that the overexpression of fusion-related genes such as *Mfn1*/*Mfn2* [25] and *Opa1* [40] induces mitochondrial elongation in MEFs. In this context, the overexpression of fission-related genes such as *Drp1* [41] and *Fis1* [42] induces mitochondrial fragmentation in MEFs and HeLa cells, respectively. However, there were only minor changes in the expression levels of *Mfn1* and *Opa1* during differentiation, and changes in the expression of *Fis1* were opposite to the expected results. Actually, FIS1 has been reported to have a weaker effect on mitochondrial fission than DNM1L in MEFs but not in HeLa [39, 41, 42] possibly due to the different mechanisms of mitochondrial morphology regulation in humans and mice. A loss-of-function experiment in a previous study showed that *Mfn1* or *Mfn2* deficiency results in fragmented mitochondrial morphology and loss of *Mfn2* has more dramatic effects than loss of *Mfn1* [25]. Moreover, OPA1, processed for mitochondrial fusion by protease isoenzymes and OMA1, might not reflect the morphology of mitochondria [43]. This is because various proteins affect the processing of OPA1 protein for its function in the mitochondrial fusion.

Next, we aimed to identify a special index that gradually increased during ESC spontaneous differentiation. We found that a gradual increase in the *Mfn2*/*Dnm1L* ratio was closely related to mitochondrial elongation during the elapsed time after the differentiation of ESCs. Additionally, we conducted correlation analysis of both *Mfn2*/*Dnm1L* and *Mfn1*/*Fis1*(one-way ANOVA with Tukey's HSD, $F = 463.54$, $p < 0.001$) ratios with mitochondrial length, because these ratios had consistent patterns like increase or decrease, respectively. Interestingly, the *Mfn2*/*Dnm1L* ($R^2 = 0.8874$) ratio pattern was more correlated with mitochondrial length than the *Mfn1*/*Fis1* ($R^2 = 0.4149$) ratio (Supplementary Fig. 3a-b). Furthermore, we found that this index could be applied to other cell types, including NSCs and MEFs. More specialized cells showed higher *Mfn2*/*Dnm1L* ratios than ESCs.

There were some limitations to our research. Firstly, technologies such as high-content imaging and machine learning were recently developed for the analysis of the shapes of mitochondria [44]. This technical method allows the analysis of the mitochondria by further subdividing the shape of the mitochondria, e.g., fragmented, rods, networks,

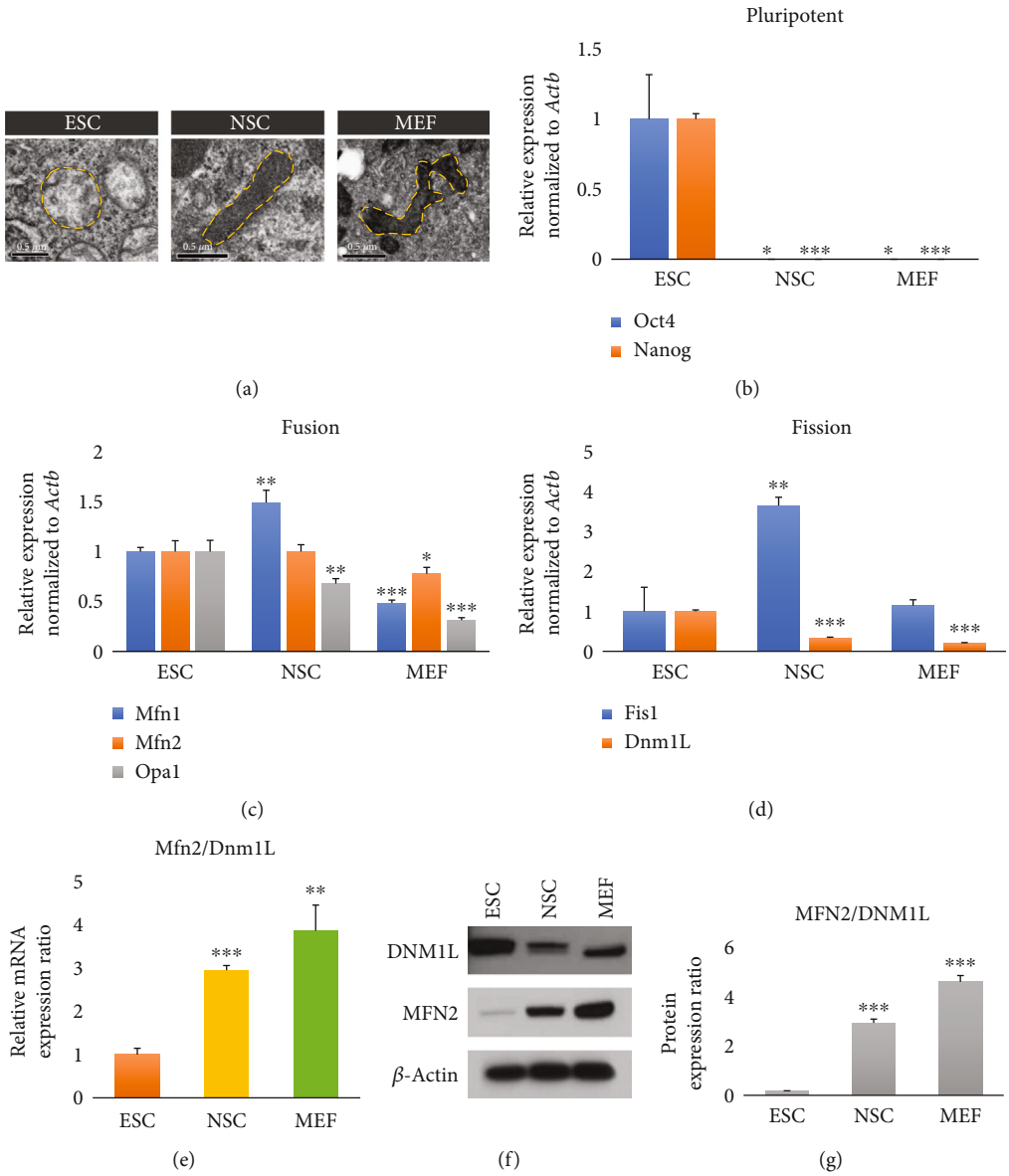

Figure 4: *Mfn2*/*Dnm1L* ratios in ESCs, NSCs, and MEFs. (a) Electron microscopic images of mitochondria in undifferentiated ESCs, NSCs, and MEFs. Yellow dotted lines represent mitochondrial morphologies. Scale bars = 0.5 μm. Quantitative RT-PCR analysis of (b) pluripotent-, (c) mitochondrial fusion-, and (d) mitochondrial fission-related genes in ESCs, NSCs, and MEFs. Gene expression levels were normalized to those of *Actb*. (e) *Mfn2*/*Dnm1L* gene expression ratios in ESCs, NSCs, and MEFs. (f) Western blotting for the expression of DNM1L and MFN2 in ESCs, NSCs, and MEFs. β-Actin was used as a control for other proteins. (g) MFN2/DNM1L protein ratios in ESCs, NSCs, and MEFs. All data are presented as mean ± SEM for $n = 3$ independent experiments. $^{*}p < 0.05$, $^{**}p < 0.01$, and $^{***}p < 0.001$ versus D0.

and large/round. However, the functions of the genes that affect the dynamic of mitochondria have yet to be identified and therefore cannot explain how mitochondria form a network [9]. Therefore, we focused on classifying the mitochondria in just two categories, i.e., fragmented and elongated. For further study, the combination of high-throughput gene screening by using RNA sequencing for sorting the gene set related to the mitochondrial dynamics will be necessary; the high-resolution imaging system with the machine learning depends on the mitochondrial morphology according to cell types. Then, we will ultimately be able to understand the various phenomena related to the shape of mitochondria and how can we regulate it. Second, some cell types at final stages of differentiation such as erythropoietic cells [45, 46] and hepatocytes [47] have fragmented mitochondria. If ESCs were differentiated by LIF withdrawal, various cell types will be observed among differentiated cell population [37, 48], including erythropoietic cells and hepatocytes. The fragmentation of mitochondria related to the specific role of cells cannot be limited to gene expression, which controls the dynamic of mitochondria. Otherwise, we showed the mitochondrial perimeter and area in Supplementary Fig. 2a-b. The error bars of these gradually expanded according to the passing of time. It means that there are various cell types which have various morphologies of mitochondria in the differentiating day 15.

Thus, the tendency of gene expression patterns can only be interpreted as the indexes that predict the degree of differentiation and shape of mitochondria, because of the random differentiation process (i.e., no lineage-specific differentiation). Thus, our findings suggested that this ratio could also be used as an index for mitochondrial morphology during differentiation.

Data Availability

The data sets used and/or analyzed during the current study are available from the corresponding author on reasonable request.

Ethical Approval

All methods used in this study were carried out in accordance with animal care and use guidelines, and all experimental protocols were approved by the Institutional Animal Care and Use Committee of Konkuk University.

Conflicts of Interest

The authors declare that they have no conflict of interest.

Authors' Contributions

JEL, BJS, KH, and JTD wrote the main manuscript text and designed the study. JEL, BJS, YJH, and MJH performed experiments and analyzed the data. JEL, BJS, HS, and JWL performed data analysis. All authors reviewed the manuscript. Jeong Eon Lee and Bong Jong Seo contributed equally to this work.

Acknowledgments

This research was supported by the Basic Science Research Program through the National Research Foundation of Korea (NRF) funded by the Ministry of Science, ICT and Future Planning of the Republic of Korea (grant nos. 2016M3A9B6946835 and 2015R15A1009701).

Supplementary Materials

Supplementary Figure 1: expression pattern of TOM20 on days 0, 3, 6, 9, 12, and 15 after differentiation of ESCs. Green dots represent mitochondria. Nuclei was counterstained with DAPI. Scale bars = 10 μm. Supplementary Figure 2: (a) the mitochondrial perimeter (μm) in ESCs on differentiating days 0, 3, 6, 9, 12, and 15. (b) The mitochondrial area (μm^2) in ESCs on differentiating days 0, 3, 6, 9, 12, and 15. Data are presented as mean ± SEM for $n = 50$ independent experiments. $^{*}p < 0.05$, $^{**}p < 0.01$, and $^{***}p < 0.001$ versus D0. Supplementary Figure 3: (a) correlation analysis between the Mfn2/Dnm1L ratio and the maximal length of mitochondria normalized to ESCs (D0). (b) Correlation analysis between the Mfn1/Fis1 ratio and the maximal length of mitochondria normalized to ESCs (D0). Supplementary Figure 4: (a) normalized protein level of DNM1L protein on days 0, 3, 6, 9, 12, and 15 after differentiation of ESCs. (b) Normalized protein level of MFN2 protein on days 0, 3, 6, 9, 12, and 15 after differentiation of ESCs. Protein expression levels were normalized to those of Actb. All data are presented as mean ± SEM for $n = 3$ independent experiments. $^{***}p < 0.001$ versus D0. *(Supplementary Materials)*

References

[1] M. G. Carter, et al.T. Hamatani, A. A. Sharov et al., "In situ-synthesized novel microarray optimized for mouse stem cell and early developmental expression profiling," *Genome Research*, vol. 13, no. 5, pp. 1011–1021, 2003.

[2] T. Hamatani, M. G. Carter, A. A. Sharov, and M. S. H. Ko, "Dynamics of global gene expression changes during mouse preimplantation development," *Developmental Cell*, vol. 6, no. 1, pp. 117–131, 2004.

[3] Q. T. Wang, et al.K. Piotrowska, M. A. Ciemerych et al., "A genome-wide study of gene activity reveals developmental signaling pathways in the preimplantation mouse embryo," *Developmental Cell*, vol. 6, no. 1, pp. 133–144, 2004.

[4] H. J. Leese, "Metabolic control during preimplantation mammalian development," *Human Reproduction Update*, vol. 1, no. 1, pp. 63–72, 1995.

[5] J. Van Blerkom, "Mitochondria in human oogenesis and preimplantation embryogenesis: engines of metabolism, ionic regulation and developmental competence," *Reproduction*, vol. 128, no. 3, pp. 269–280, 2004.

[6] C.. D. L. Folmes, P.. P. Dzeja, T.. J. Nelson, and A. Terzic, "Metabolic plasticity in stem cell homeostasis and differentiation," *Cell Stem Cell*, vol. 11, no. 5, pp. 596–606, 2012.

[7] H. W. Choi, et al.J. H. Kim, M. K. Chung et al., "Mitochondrial and metabolic remodeling during reprogramming and differentiation of the reprogrammed cells," *Stem cells and Development*, vol. 24, no. 11, pp. 1366–1373, 2015.

[8] A. D. Panopoulos, et al.O. Yanes, S. Ruiz et al., "The metabolome of induced pluripotent stem cells reveals metabolic changes occurring in somatic cell reprogramming," *Cell Research*, vol. 22, no. 1, pp. 168–177, 2012.

[9] B. Seo, S. Yoon, and J. Do, "Mitochondrial dynamics in stem cells and differentiation," *International journal of molecular Sciences*, vol. 19, no. 12, p. 3893, 2018.

[10] D. F. Suen, K. L. Norris, and R. J. Youle, "Mitochondrial dynamics and apoptosis," *Genes & Development*, vol. 22, no. 12, pp. 1577–1590, 2008.

[11] A. Bratic and N. G. Larsson, "The role of mitochondria in aging," *The Journal of Clinical Investigation*, vol. 123, no. 3, pp. 951–957, 2013.

[12] A. Wanet, T. Arnould, M. Najimi, and P. Renard, "Connecting mitochondria, metabolism, and stem cell fate," *Stem Cells and Development*, vol. 24, no. 17, pp. 1957–1971, 2015.

[13] B. Westermann, "Bioenergetic role of mitochondrial fusion and fission," *Biochimica et Biophysica Acta*, vol. 1817, no. 10, pp. 1833–1838, 2012.

[14] Y. M. Cho, et al.S. Kwon, Y. K. Pak et al., "Dynamic changes in mitochondrial biogenesis and antioxidant enzymes during the spontaneous differentiation of human embryonic stem cells," *Biochemical and Biophysical Research Communications*, vol. 348, no. 4, pp. 1472–1478, 2006.

[15] H. Chen and D. C. Chan, "Mitochondrial dynamics in mammals," *Current Topics in Developmental Biology*, vol. 59, pp. 119–144, 2004.

[16] D. C. Chan, "Mitochondrial fusion and fission in mammals," *Annual Review of Cell and Developmental Biology*, vol. 22, no. 1, pp. 79–99, 2006.

[17] W. Fu, Y. Liu, and H. Yin, "Mitochondrial dynamics: biogenesis, fission, fusion, and mitophagy in the regulation of stem cell behaviors," *Stem Cells International*, vol. 2019, Article ID 9757201, 15 pages, 2019.

[18] J. C. St. John, J. Ramalho-Santos, H. L. Gray et al., "The expression of mitochondrial DNA transcription factors during early cardiomyocyte in vitro differentiation from human embryonic stem cells," *Cloning and Stem Cells*, vol. 7, no. 3, pp. 141–153, 2005.

[19] S. Chung, P. P. Dzeja, R. S. Faustino, C. Perez-Terzic, A. Behfar, and A. Terzic, "Mitochondrial oxidative metabolism is required for the cardiac differentiation of stem cells," *Nature Clinical Practice. Cardiovascular Medicine*, vol. 4, Suppl 1, pp. S60–S67, 2007.

[20] H. Kondoh, et al.M. E. Lleonart, Y. Nakashima et al., "A high glycolytic flux supports the proliferative potential of murine embryonic stem cells," *Antioxidants & Redox Signaling*, vol. 9, no. 3, pp. 293–299, 2007.

[21] T. Lonergan, B. Bavister, and C. Brenner, "Mitochondria in stem cells," *Mitochondrion*, vol. 7, no. 5, pp. 289–296, 2007.

[22] K. Okamoto and J. M. Shaw, "Mitochondrial morphology and dynamics in yeast and multicellular eukaryotes," *Annual Review of Genetics*, vol. 39, no. 1, pp. 503–536, 2005.

[23] B. Westermann, "Mitochondrial fusion and fission in cell life and death," *Nature Reviews Molecular Cell Biology*, vol. 11, no. 12, pp. 872–884, 2010.

[24] A. Santel and M. T. Fuller, "Control of mitochondrial morphology by a human mitofusin," *Journal of Cell Science*, vol. 114, pp. 867–874, 2001.

[25] H. Chen, S. A. Detmer, A. J. Ewald, E. E. Griffin, S. E. Fraser, and D. C. Chan, "Mitofusins Mfn1 and Mfn2 coordinately regulate mitochondrial fusion and are essential for embryonic development," *The Journal of Cell Biology*, vol. 160, no. 2, pp. 189–200, 2003.

[26] C. Delettre, et al.G. Lenaers, J. M. Griffoin et al., "Nuclear gene _OPA1_ , encoding a mitochondrial dynamin-related protein, is mutated in dominant optic atrophy," *Nature Genetics*, vol. 26, no. 2, pp. 207–210, 2000.

[27] S. Meeusen, et al.R. DeVay, J. Block et al., "Mitochondrial inner-membrane fusion and crista maintenance requires the dynamin-related GTPase Mgm1," *Cell*, vol. 127, no. 2, pp. 383–395, 2006.

[28] Z. Song, M. Ghochani, J. M. McCaffery, T. G. Frey, and D. C. Chan, "Mitofusins and OPA1 mediate sequential steps in mitochondrial membrane fusion," *Molecular Biology of the Cell*, vol. 20, no. 15, pp. 3525–3532, 2009.

[29] N. Ishihara, Y. Fujita, T. Oka, and K. Mihara, "Regulation of mitochondrial morphology through proteolytic cleavage of OPA1," *The EMBO Journal*, vol. 25, no. 13, pp. 2966–2977, 2006.

[30] O. S. Shirihai, M. Song, and G. W. Dorn II, "How mitochondrial dynamism orchestrates mitophagy," *Circulation Research*, vol. 116, no. 11, pp. 1835–1849, 2015.

[31] Y. Zhang and D. C. Chan, "Structural basis for recruitment of mitochondrial fission complexes by Fis1," *Proceedings of the National Academy of Sciences of the United States of America*, vol. 104, no. 47, pp. 18526–18530, 2007.

[32] Y. Yoon, E. W. Krueger, B. J. Oswald, and M. A. McNiven, "The mitochondrial protein hFis1 regulates mitochondrial fission in mammalian cells through an interaction with the dynamin-like protein DLP1," *Molecular and Cellular Biology*, vol. 23, no. 15, pp. 5409–5420, 2003.

[33] D. I. James, P. A. Parone, Y. Mattenberger, and J. C. Martinou, "hFis1, a novel component of the mammalian mitochondrial fission machinery," *The Journal of Biological Chemistry*, vol. 278, no. 38, pp. 36373–36379, 2003.

[34] E. Smirnova, D. L. Shurland, S. N. Ryazantsev, and A. M. van der Bliek, "A human dynamin-related protein controls the distribution of mitochondria," *The Journal of Cell Biology*, vol. 143, no. 2, pp. 351–358, 1998.

[35] D. Otsuga, et al.B. R. Keegan, E. Brisch et al., "The dynamin-related GTPase, Dnm1p, controls mitochondrial morphology in yeast," *The Journal of Cell Biology*, vol. 143, no. 2, pp. 333–349, 1998.

[36] A. Legesse-Miller, R. H. Massol, and T. Kirchhausen, "Constriction and Dnm1p recruitment are distinct processes in mitochondrial fission," *Molecular Biology of the Cell*, vol. 14, no. 5, pp. 1953–1963, 2003.

[37] M. Y. Cherepkova, G. S. Sineva, and V. A. Pospelov, "Leukemia inhibitory factor (LIF) withdrawal activates mTOR signaling pathway in mouse embryonic stem cells through the MEK/ERK/TSC2 pathway," *Cell death & disease.*, vol. 7, no. 1, p. e2050, 2016.

[38] Z. Zhang, L. Liu, S. Wu, and D. Xing, "Drp1, Mff, Fis1, and MiD51 are coordinated to mediate mitochondrial fission during UV irradiation-induced apoptosis," *The FASEB Journal*, vol. 30, no. 1, pp. 466–476, 2016.

[39] O. C. Losón, Z. Song, H. Chen, and D. C. Chan, "Fis1, Mff, MiD49, and MiD51 mediate Drp1 recruitment in mitochondrial fission," *Molecular Biology of the Cell*, vol. 24, no. 5, pp. 659–667, 2013.

[40] C. Frezza, S. Cipolat, and L. Scorrano, "Measuring mitochondrial shape changes and their consequences on mitochondrial involvement during apoptosis," in *Methods in Molecular Biology*, vol. 372, pp. 405–420, Humana Press, 2007.

[41] T. Yamamori, et al.S. Ike, T. Bo et al., "Inhibition of the mitochondrial fission protein dynamin-related protein 1 (Drp1) impairs mitochondrial fission and mitotic catastrophe after x-irradiation," *Molecular Biology of the Cell*, vol. 26, no. 25, pp. 4607–4617, 2015.

[42] H. Otera, C. Wang, M. M. Cleland et al., "Mff is an essential factor for mitochondrial recruitment of Drp1 during mitochondrial fission in mammalian cells," *The Journal of Cell Biology*, vol. 191, no. 6, pp. 1141–1158, 2010.

[43] S. Ehses, I. Raschke, G. Mancuso et al., "Regulation of OPA1 processing and mitochondrial fusion by m-AAA protease isoenzymes and OMA1," *The Journal of Cell Biology*, vol. 187, no. 7, pp. 1023–1036, 2009.

[44] A. P. Leonard, R. B. Cameron, J. L. Speiser et al., "Quantitative analysis of mitochondrial morphology and membrane potential in living cells using high-content imaging, machine learning, and morphological binning," *Biochimica et Biophysica Acta (BBA)-Molecular Cell Research*, vol. 1853, no. 2, pp. 348–360, 2015.

[45] X. Liu, Y. Zhang, M. Ni et al., "Regulation of mitochondrial biogenesis in erythropoiesis by mTORC1-mediated protein translation," *Nature cell Biology*, vol. 19, no. 6, pp. 626–638, 2017.

[46] E. L. Jensen, A. M. Gonzalez-Ibanez, P. Mendoza et al., "Copper deficiency-induced anemia is caused by a mitochondrial

metabolic reprograming in erythropoietic cells," *Metallomics*, vol. 11, no. 2, pp. 282–290, 2019.

[47] S. Das, N. Hajnóczky, A. N. Antony et al., "Mitochondrial morphology and dynamics in hepatocytes from normal and ethanol-fed rats," *Pflügers Archiv-European Journal of Physiology*, vol. 464, no. 1, pp. 101–109, 2012.

[48] D. Duval, B. Reinhardt, C. Kedinger, and H. Boeuf, "Role of suppressors of cytokine signaling (Socs) in leukemia inhibitory factor (LIF)-dependent embryonic stem cell survival," *The FASEB Journal*, vol. 14, no. 11, pp. 1577–1584, 2000.